Check for updates

View Article Online
View Journal

Soft Matter

Accepted Manuscript

This article can be cited before page numbers have been issued, to do this please use: E. Moghimi, A. Jacob and G. Petekidis, *Soft Matter*, 2017, DOI: 10.1039/C7SM01655G.

This is an Accepted Manuscript, which has been through the Royal Society of Chemistry peer review process and has been accepted for publication.

Accepted Manuscripts are published online shortly after acceptance, before technical editing, formatting and proof reading. Using this free service, authors can make their results available to the community, in citable form, before we publish the edited article. We will replace this Accepted Manuscript with the edited and formatted Advance Article as soon as it is available.

You can find more information about Accepted Manuscripts in the author guidelines.

Please note that technical editing may introduce minor changes to the text and/or graphics, which may alter content. The journal's standard Terms & Conditions and the ethical guidelines, outlined in our author and reviewer resource centre, still apply. In no event shall the Royal Society of Chemistry be held responsible for any errors or omissions in this Accepted Manuscript or any consequences arising from the use of any information it contains.

ROYAL SOCIETY OF CHEMISTRY

rsc.li/soft-matter-journal

View Article Online
DOI: 10.1039/C7SM01655G

Journal Name

ARTICLE TYPE

Cite this: DOI: 10.1039/xxxxxxxxxx

Residual Stresses in Colloidal Gels†

Esmaeel Moghimi,[a] Alan R. Jacob [a,b] and George Petekidis *[a]

Received Date
Accepted Date

DOI: 10.1039/xxxxxxxxxx

www.rsc.org/journalname

A combination of experiments and Brownian Dynamics (BD) simulations is utilized to examine internal stresses in colloidal gels brought to rest from steady shear at different shear rates. A model colloidal gel with intermediate volume fraction is chosen where attractions between particles are introduced by adding non-adsorbing linear polymer chains. After flow cessation, the gel releases the stress in two distinct patterns: At high shear rates, where shear forces dominate over attractive forces, the shear-melted gel behaves as a liquid and releases stresses to zero after flow cessation. After low shear rates, though, stresses relax only partially, similar to the response of hard sphere glasses and jammed soft particles. The balance between shear and attractive forces which determines the intensity of structural distortion controls the amplitude of the residual stresses through a universal scaling. Stress decomposition to repulsive and attractive contributions in BD simulations reveals that internal stresses are mainly originating from attractive forces. Moreover, analysis of particle dynamics indicate that internal stresses are associated to sub-diffusive particle displacements on average smaller than the attraction range as such short-range displacements are not sufficient enough to completely erase structural anisotropy caused during the course of shear.

1 Introduction

Colloidal dispersions are widely present in daily life products such as milk, inks, paints, mayonnaise as well as in a variety of biological systems[1]. These materials often are soft yield-stress viscoelastic fluids, i.e., they exhibit solid-like response at low stresses. However, they may yield and flow when large enough stresses (or strains) are imposed. After quenching such materials from a flowing liquid state to the solid state at rest, a part of the stress stored during flow (or shear) will remain since the structure is not able to relax instantaneously. These stresses are referred to as residual stresses. In general, residual stresses have been observed during cooling of polymer melts[2], temperature jumps in multilamellar vesicle suspensions[3–5], reconstitution of actin networks[6], dewetting of thin polymeric films[7], drying of concentrated colloidal suspensions[8] and after flow cessation of colloidal systems such as hard sphere glasses[9], jammed soft particle suspensions[10,11], dilute gels of fumed silica particles[12,13] and laponite particle gels[14]. However, one should distinguish internal stresses developed by shear cessation from the contractile internal stresses that arise through thermal quenching from a liquid state. In the former, internal stresses are anisotropic and originate from the persistence of the structural anisotropy caused during the shear[9–11] while in the latter they are isotropic and are caused by structural arrest en-route to the equilibrium state[15–17]. Moreover, the relaxation of residual stresses built-up during quenching from liquid to solid state have been invoked to explain the slow dynamics and aging of disordered soft solids[3–6,17]. Internal stresses were also found to be responsible for undesirable rupture of thin polymeric films although such systems were expected to be energetically stable[7]. Furthermore, if internal stresses are tuned properly, they can improve mechanical properties of material as found in silicate[18] and metallic glasses[19,20]. Similarly, residual stresses in suspensions of colloidal hard spheres can be tuned by the particle volume fraction and the preshear history[9]. The larger the preshear rate, the smaller the ratio of internal stress to that developed before shear cessation. A similar finding has also been reported in suspensions of jammed soft particles where the persistence of the asymmetric angular distortions which characterize the pair distribution function during flow were identified as their microscopic origin[10,11]

However, the underlying mechanisms, relating residual stresses with the microscopic structure and particle dynamics in model soft matter systems with interparticle attractions are not well un-

[a] FORTH/IESL and Department of Materials Science and Technology, University of Crete, 71110 Heraklion, Greece. E-mail: georgp@iesl.forth.gr
[b] Current address: North Carolina State University, Raleigh, NC 27695, USA

† Electronic Supplementary Information (ESI) available: [details of any supplementary information available should be included here]. See DOI: 10.1039/b000000x/

‡ Additional footnotes to the title and authors can be included *e.g.* 'Present address:' or 'These authors contributed equally to this work' as above using the symbols: ‡, §, and ¶. Please place the appropriate symbol next to the author's name and include a `\footnotetext` entry in the the correct place in the list.

Published on 05 October 2017. Downloaded by University of Newcastle on 08/10/2017 18:22:05.

Soft Matter Accepted Manuscript

View Article Online
DOI: 10.1039/C7SM01655G

Published on 05 October 2017. Downloaded by University of Newcastle on 08/10/2017 18:22:05.

derstood. One such model system is a mixture of hard sphere colloids with nonadsorbing linear polymer chains as depletants where the strength and range of interparticle attraction are tuned by the concentration and size of polymer chains, respectively[21,22].

Colloidal gels at intermediate volume fraction ($0.2 < \phi < 0.5$) and attractive glasses show complex response to shear with yielding in two-step process related to an initial short scale bond breaking and larger scale cage/cluster melting[23–28]. The application of shear in such colloidal gels has been demonstrated to strongly alter the structure and mechanical properties during and after flow cessation[28,29]. Depending on the shear rate, bond breaking or cluster formation/densification under shear takes place[28–38].

In this paper, we use a combination of rheological experiments and BD simulations in order to understand the link between stresses, structure and dynamics after flow cessation of steady state shear flow in a model system of colloid-polymer depletion gel at intermediate volume fraction ($\phi = 0.44$). We demonstrate that depending on the applied shear rate, such colloidal gels release internal stresses in two distinct patterns, after flow cessation: At high shear rates, stresses are released quickly, similarly to what is seen in liquids, as particles can easily move to achieve new configurations with reduced internal stresses, while at low shear rates, stresses decay only partially as in hard sphere colloidal glasses. The balance between shear and attractive forces, which determines the intensity of structural distortion under shear, controls the amount of the residual stresses through a universal scaling.

The paper is structured as follows: In section 2, we present the materials used in the study and the techniques of experimental rheology and BD simulations. In the results and discussion section 3, we first discuss the stresses and structures under steady shear flow and then after shear cessation, in sections 3.1 and 3.2 , respectively. Then, we present the structural anisotropy caused by shear in section 3.3 and we explain particle scale dynamics in section 3.4 and scaling of residual stresses in section 3.5 before ending with the conclusions in section 4.

2 Materials and methods

We used nearly hard-sphere polymethylmethacrylate (PMMA) particles sterically stabilized by chemically grafted poly-hydroxy-stearic acid (PHSA) chains (~ 10 nm) dispersed in octadecene. Particles have hydrodynamic radius of $R = 400$ nm (measured in dilute suspensions by dynamic light scattering). Depletion attractions were implemented between particles by adding non-adsorbing linear polybutadiene (1, 4-addition) with molecular weight, $M_w = 1243300$ g/mol and a radius of gyration, $R_g = 34$ nm (measured by static light scattering). This implies a polymer-colloid size ratio $\xi = R_g/R = 0.09$ in dilute solution. We prepared the gel at an intermediate particle volume fraction, $\phi = 0.44$, and polymer concentration, $c_p = 0.0046$ g/cm^3. The latter gives an attraction strength at contact $U_{dep}(2R) = -20k_BT$ according to the modified Asakura-Oosawa (AO) model[21,39]. It should be noticed that according to Generalized Free Volume Theory (GFVT)[40] in dense suspensions, the effective polymer-colloid size ratio and the corresponding attraction strength at contact are reduced to $\xi^* = 0.06$ and $U_{dep}(2R) = -13.1k_BT$, respectively. Note that in all figure captions presented here, we report the nominal values from the AO potential.

In order to examine the scaling law for residual stresses and to explore lower Pe regime, we used smaller particles with radius $R = 196$ nm dispersed in octadecene with non-adsorbing linear polybutadiene (1, 4-addition) with molecular weight, $M_w = 323000$ g/mol and a radius of gyration, $R_g = 19$ nm. This gives a polymer-colloid size ratio $\xi = R_g/R = 0.1$ in dilute solution. The gel prepared at volume fraction $\phi = 0.44$ and polymer concentrations, $c_p = 0.0027$ and 0.0076 g/cm^3 which imply attraction strengths at contact of $U_{dep}(2R) = -6$ and $-20k_BT$, respectively according to modified AO[21,39].

Rheological experiments were performed with an Anton-Paar MCR 501 rheometer with homemade cone-plate geometries of diameter 25 mm, cone angle 2.7° and cone truncation 0.05 mm with roughened surfaces to avoid wall-slip[37]. By using these serrated geometries, we did not detect wall-slip under shear as is evidenced by the absence of a second pseudo-yield stress plateau at low shear rates in the flow curve in agreement with previous results[37]. Moreover, no indication of wall slip due to sedimentation and gel collapse was observed in the linear viscoelastic moduli after long term aging[37]. Temperature was set to $T = 20$ $^\circ C$ using a standard Peltier plate with a solvent saturation trap to minimize evaporation, although octadecene due to high boiling point (b.p. 315 ^oC) does not evaporate for several days at room temperature.

We also performed Brownian Dynamics (BD) simulations to get both rheological and detailed structural information similar with previous studies[25,28,29,41,42] . Affine shear was applied on 30000 particles (with 10% polydispersity to avoid crystallization) with periodic boundary conditions. Hard-sphere interactions in BD simulations are introduced by using a potential-free algorithm which corrects the overlap between pairs of particles by moving them back to contact with the equal force along the line of centers[43]. In this method, HS stresses are determined through calculating the pairwise interparticle forces that would have resulted in the hard sphere displacements during the course of a time step[44]. In this case, the HS forces are the average Stokes drag on the particle during the course of the HS displacement ($F^{HS} = 6\pi\eta R\frac{\Delta x^{HS}}{\Delta t}$). Depletion attractions are implemented in simulations by using AO potential[21] which is expected to mimic the experimental system of hard sphere colloids and linear polymer mixture. The potential, $U_{dep}(r) = \Pi V_{overlap}(r)$, is the product of the osmotic pressure and the overlap volume which changes for each pair of particles. BD simulations were performed at a constant attraction range of $\xi = 0.1$ and various attraction strengths at contact of -10, -20 and -50k_BT. We modified AO potential near the point of contact and at a distance of $\xi_g = 0.01R$ to implement a constant potential. The reason for such modification was to approach the experimental conditions by introducing a small amount of interparticle flexibility, without modifying the basic hard sphere algorithm[28]. The stresses due to the depletion are calculated from the particle positions and forces in each time step as $\sigma^{Dep} = \frac{\Sigma \vec{r}.\vec{F}^{Dep}}{V}$ where $F^{Dep} = \frac{dU}{dr}$ is the depletion force. The overall stress response is the sum of the hard sphere interac-

Soft Matter Accepted Manuscript

This journal is © The Royal Society of Chemistry [year]

View Article Online
DOI: 10.1039/C7SM01655G

Published on 05 October 2017. Downloaded by University of Newcastle on 08/10/2017 18:22:05.

tion stresses and the additional stresses due to depletion forces: $\sigma = \sigma^{HS} + \sigma^{Dep}$.

The internal time scales in BD simulations and experiments are expected to be different due to lack of hydrodynamic interactions in the former. As in real systems particle diffusion (both short- and long-time) is volume fraction dependent due to hydrodynamic interactions, the Brownian relaxation time in experiments is expected to be increased by about an order of magnitude (compared to the free dilute limit)[45], due to the existence of concentrated glassy clusters, similarly with HS glasses. Thus, we multiply the Brownian time-scale in experiments $t_B(=\frac{6\pi\eta R^3}{k_BT} = 1.25s$ with $\eta = 4.2mPa.s$ being the solvent viscosity) and non-dimensional shear rate $Pe(=\dot{\gamma}t_B)$ by a factor of 10 in all figures. Note, however, this is just a rough approximation allowing a more realistic comparison between experiments and BD simulations.

2.1 Analysis of structural anisotropy

We examine structural anisotropy through expanding the pair distribution function $g(r)$ into an orthogonal series of spherical harmonic functions $Y_l^m(\theta,\phi)$ (of the degree l and order m of the spherical coordinates θ and ϕ)[46–48]:

$$g(\vec{r}) = g_s(r) + \sum_{l=0}^{\infty}\sum_{m=-l}^{l} g_l^m(r) Y_l^m(\theta,\phi) \quad (1)$$

where $g_s(r)$ is the scaler contribution:

$$g_s(r) = \frac{1}{4\pi}\int g(\vec{r})d\hat{r} \quad (2)$$

with $\hat{r} = \frac{\vec{r}}{r}$ and $d\hat{r}$ being the solid angle element (often denoted also as $d\Omega$). $g_l^m(r)$ is the expansion coefficient $(=\int Y_l^m(\theta,\phi)g(\vec{r})d\hat{r})$ providing information on the structural anisotropy. Application of a steady shear flow in colloidal dispersions causes an asymmetry in the angular dependence of the pair distribution function due to accumulation and depletion of particles in the compression and extension axes, respectively. Such shear-induced structural anisotropy is quantified by the expansion coefficient $g_2^{-2}(r)$. For a simple shear flow, $g_2^{-2}(r)$ is calculated as follows[10,11,49–52]:

$$g_2^{-2}(r) = \frac{15}{4\pi}\int \hat{x}\hat{y}g(\vec{r})d\hat{r} \quad (3)$$

where $\hat{x}$ and $\hat{y}$ are the Cartesian components of $\hat{r}$. In this case, the corresponding shear stress, σ_{xy} , generated from such shear-induced structural anisotropy in the velocity-gradient (xy) plane can be calculated as[47]:

$$\sigma_{xy} = -\frac{2}{15}\pi\rho^2\int_0^{\infty} r^3\frac{dU}{dr}g_2^{-2}(r)dr \quad (4)$$

where ρ is the particle number density and $\frac{dU}{dr}$ is the derivative of interparticle potential (or the magnitude of interparticle force). Note, that the equivalent stress for HS suspensions can be calculated as $\sigma_{xy} = -\rho^2 k_BTR(2R)^2 g_0(2R)\int\hat{x}\hat{y}fd\hat{r}$ where f represents the deviation of $g(r)$ from equilibrium[25,44,53].

3 Results and Discussion

3.1 Steady state shear flow

In order to explain the different macromechanical and microstructural responses detected under shear and also the transition from low to high shear rates, we use the ratio of Stokes drag to depletion attraction forces, defined by Koumakis et al.[29] as the dimensionless number, Pe_{dep}, (note this is the same with $M^{'}$ defined by Eberle et al.[54] and Kim et al.[55]):

$$Pe_{dep} = \frac{F_{shear}}{F_{dep}} = \frac{6\pi\eta R(2\xi R)}{U_{dep}(2R)/(2\xi R)}\frac{\dot{\gamma}}{2\xi} = \frac{12\pi\eta\xi R^3\dot{\gamma}}{U_{dep}(2R)} \quad (5)$$

For values of $Pe_{dep} > 1$ shear forces are stronger than attractive forces and bond breaking under shear is expected to take place, whereas for $Pe_{dep} < 1$ attractive forces dominate over shear forces. In the latter regime, shear assists particles to rearrange locally and find a lower minimum in the energy landscape as has been seen both under steady[29] and oscillatory[28] shear flows.

In **Fig.** 1, we present the steady state shear stress as a function of shear rate (flow curve) from both experiments and BD simulations. The flow curve exhibits the expected typical response for colloidal gels. For values of $Pe_{dep} >> 1$ ($Pe >> 100$), there is a linear relation between stress and shear rate indicative of viscous flow with constant viscosity. For $Pe_{dep} < 1$, we get a sub-linear relation which indicates shear-thinning behavior and at very low Pe_{dep}, a yield stress plateau emerges. Such macromechanical response is directly connected to shear-induced structural changes at microscopic level. The 2D images of the structure under shear from BD simulations are also shown in **Fig.** 1. Particles are colored according to the number of neighboring particles within the attraction range, which defines a bond. A detailed quantitative description of bonds distribution will be presented in the following section. Shearing at high rates ($Pe_{dep} > 1$) breaks all bonds between particles and results into formation of relatively homogeneous structures similar to a HS liquid at equivalent volume fraction, flowing with a simple viscous response under shear. Conversely, shearing at low rates (at $Pe_{dep} < 1$) leads to the formation of highly heterogeneous structures with dense clusters that decrease in size with increasing shear rate; this subsequently leads to less resistance against flow and thus a decrease of effective viscosity (shear-thinning response). Therefore, depending on Pe, two distinct regimes are detected under shear as has been presented before[29]. One where clusters break-up at high shear rates ($Pe_{dep} > 1$) and the another where clusters densify at low shear rates ($Pe_{dep} < 1$). It is therefore interesting to investigate how the gel will release stresses in these two regimes of shear when flow is stopped.

3.2 Flow cessation

In **Fig.** 2, we present the stress decay with time after flow cessation of the steady shear at different shear rates from both experiments and BD simulations. In order to see the short time response and the transition from liquid-like to solid-like behavior clearly, we plot the stress decay in log-log scale. **Fig.** 2**a** shows

Soft Matter Accepted Manuscript

View Article Online
DOI: 10.1039/C7SM01655G

Published on 05 October 2017. Downloaded by University of Newcastle on 08/10/2017 18:22:05.

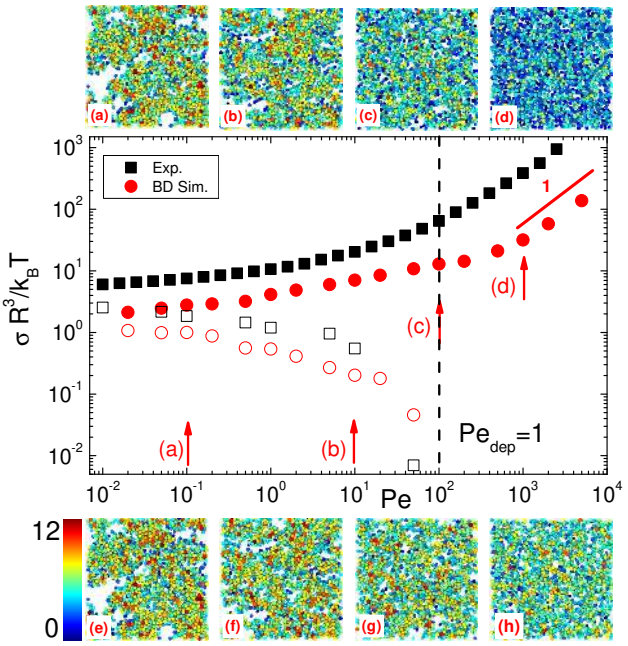

Fig. 1 Normalized stresses as a function of Pe (flow curve) from experiments (solid black squares) and BD simulations (solid red circles). Residual stresses at $10t_B$ after flow cessation are indicated from experiments (open black squares) and BD simulations (open red circles). Vertical dashed line represents $Pe_{dep} = 1$. Top images are structures under shear taken from BD simulations (rates indicated by arrows). Bottom images are the corresponding structures at $10t_B$ after flow cessation. Particles are colored by the number of bonds. For experiments, $U_{dep}(2R) = -20k_BT$, $\xi = 0.09$, $Pe/Pe_{dep} = 110$ and for simulations, $U_{dep}(2R) = -20k_BT$, $\xi = 0.1$, $Pe/Pe_{dep} = 100$.

the results from experiments. Two distinct patterns of stress decay are observed. After flow cessation at high shear rates, the stress is released quickly and relaxes completely to zero similarly to what has been observed in HS liquids[9]. For low shear rates, however, the stress relaxes partially as in HS colloidal glasses and jammed soft particles[9,10]. With increasing shear rate, the amount of residual stresses decreases in absolute values (**Fig. 2 a** and **b**). In **Fig. 2b**, we present the results from BD simulations. There is a qualitative agreement between experiments and BD simulations: At high Pe, we detect a complete relaxation of stress while at low Pe the stress relaxes to a plateau or is slowly decreasing towards zero (or to a finite lower frozen stress). However, there seems to be a quantitative difference between experiments and simulations: in experiments the transition from fully to partially relaxing decay seems to be more abrupt (between $Pe = 10$ and 50) while in BD simulations there is a power law decrease of the stress for $Pe = 10$ to 100 with no clear transition. One should notice that in BD simulations flow cessation at high shear rates ($Pe = 1000$) shows an initial stress response similar to liquids although at long times after the system has reached steady state relaxation, we detect negative shear stress values (see **Fig. 3 c**). We address this issue in more details later when we examine the structural anisotropy caused by shear.

The close agreement between BD simulations and rheological experiments provides strong justification for the use of BD simulations to extract valuable structural information at the microscopic level, that may reveal the underlying mechanisms of such stress decay. Moreover, as both in experiments and BD simulations the stress decays slowly over time, it would be interesting to see if after very long times the stress completely relaxes as has been found in jammed microgel suspensions[11], although this calls for more extensive experiments and BD simulations which both are technically quite demanding. The two distinct patterns of stress decay, i.e., the liquid-like response after high shear rates and solid-like response observed after flow cessation of low shear rates should result from different microstructural mechanisms, i. e., may be linked with the cluster break-up at high shear rates and cluster densification at low shear rates[29]. In **Fig. 1**, we plot the residual stresses at $10t_B$ after flow cessation for different shear rates together with the flow curve. Remarkably, the transition from liquid-like to solid-like response occurs around $Pe_{dep} = 1$. For $Pe_{dep} > 1$, where shear forces are stronger than attractive forces and cluster break-up under shear takes place, there are no detectable residual stresses both in experiments and BD simulations, as the system immediately after shear cessation is found in a liquid state with particles dispersed homogeneously. In contrast, for $Pe_{dep} < 1$ where cluster densification under shear occurs, significant residual stresses are measured after shear cessation which decay only slowly over time. As we are getting closer to yield stress plateau, residual stresses increase. These results emphasize the importance of performing a shear rejuvenation at high shear rates where $Pe_{dep} >> 1$ in order to completely release the internal stresses and erase the history effects. Furthermore, for more complex attractive systems, one way to find the shear rate at which $Pe_{dep} = 1$ could be achieved by performing stress relaxation experiments at different shear rates and detecting the shear rate at which a transition from liquid-like to solid-like response takes place. If we normalize the stress by the steady shear value before flow cessation and scale the time with the shear rate, for both experiments and BD simulations all relaxation curves at intermediate times collapse (**Fig. 2c** and **d**) similarly to HS colloidal glasses[9]. In the case of glasses, this scaling is attributed to the slow decay of structural anisotropy at the level of the first neighbors as detected in the pair distribution function[9].

3.2.1 Stress decomposition to HS and depletion contributions:

As discussed in section 2, the overall stresses in BD simulations are the sum of contributions from hard-sphere and attractive stresses. In **Fig. 3**, we show the decomposition of the overall stresses of **Fig. 2 b** into repulsive and attractive stresses. This may characterize the nature of the relaxation in terms of two contributions, the hard sphere potential and the depletion attractive potential. We examine three regimes, one for $Pe_{dep} < 1$ where cluster densification under shear takes place, the second for $Pe_{dep} = 1$ and finally for $Pe_{dep} > 1$ where cluster break-up is the most dominant microscopic mechanism. For the low Pe ($= 0.1$) corresponding to $Pe_{dep} = 0.001$ (**Fig.3 a**), both HS and attractive stresses are contributing positively to the overall stress and decay over time. HS stresses relax over time almost to zero while attractive stresses reach a constant value at long times ($10t_B$) after shear cessation.

Soft Matter Accepted Manuscript

This journal is © The Royal Society of Chemistry [year]

View Article Online
DOI: 10.1039/C7SM01655G

Published on 05 October 2017. Downloaded by University of Newcastle on 08/10/2017 18:22:05.

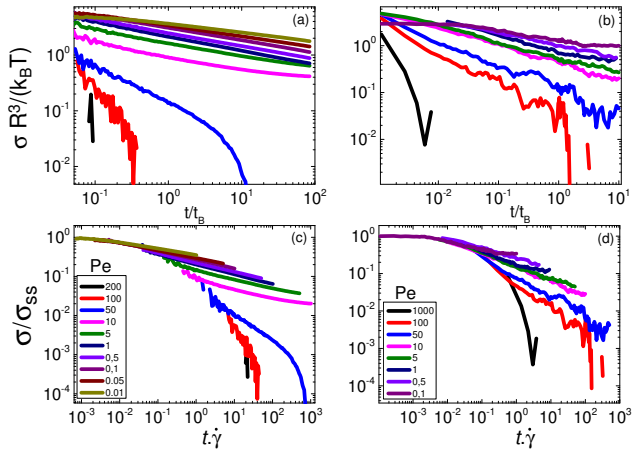

Fig. 2 Stress relaxation after flow cessation at different steady shear rates as indicated for (a) experiments and (b) BD simulations. (c) and (d) correspond to data from (a) and (b), respectively, with the stress normalized with the steady state value and the time scaled with the shear rate prior to shear cessation with (c) experiments and (d) BD simulations. For experiments, $\phi = 0.44$, $U_{dep}(2R) = -20k_BT$, $\xi = 0.09$, $Pe/Pe_{dep} = 110$ and simulations, $\phi = 0.44$, $U_{dep}(2R) = -20k_BT$, $\xi = 0.1$, $Pe/Pe_{dep} = 100$.

Hence, residual stresses here are mainly originating from the attractive forces. For $Pe = 100$ (corresponding to $Pe_{dep} = 1$) (**Fig. 3b**), we find that stresses due to depletion attractions are positively contributing to the overall stress, while HS stresses are negative with the same more or less absolute values. This leads to a net zero value of the overall stress. Finally, for the strong Pe ($= 1000$ corresponding to $Pe_{dep} = 10$) (**Fig. 3 c**), the sign of stresses are reversed. HS stresses are positive and show a decay over time, while depletion ones are negative with larger absolute values and show an increase over time. This leads to the negative value of the overall stress. Such rich shear rate dependent stress response is explained in detail through the examination of the structural changes caused by shear both during steady shear and after flow cessation using BD simulations.

In previous studies, we have extensively discussed the microstructural changes taking place during flow and after shear cessation for both steady[29] and oscillatory[28] shear flows. Here, we briefly discuss the main findings. The structure is characterized by calculating the void volume, VV, and the average number of bonds per particle. The void volume is defined as the volume of the sphere with the center in the empty space and the radius equals to the closest particle distance. Mapping VV provides information on the distribution of void volumes. **Fig. 4a** shows the distribution of void volume under steady shear of varying Pe. The gel under sufficiently large shear rates ($Pe_{dep} > 1$) exhibits smaller void volumes with a rather narrow distribution. This reflects a homogeneous distribution of particles with an average distance of the order of, or smaller than, $2R$, as expected from a liquid HS suspension with similar volume fraction ($\phi = 0.44$). In contrast, for low Pe ($Pe_{dep} < 1$), the VV distribution shows two broad peaks/shoulders indicating the bimodal distributions of length scales with the first peak taking place at length scales comparable to the attraction range (of $\xi = 0.1$) while the second

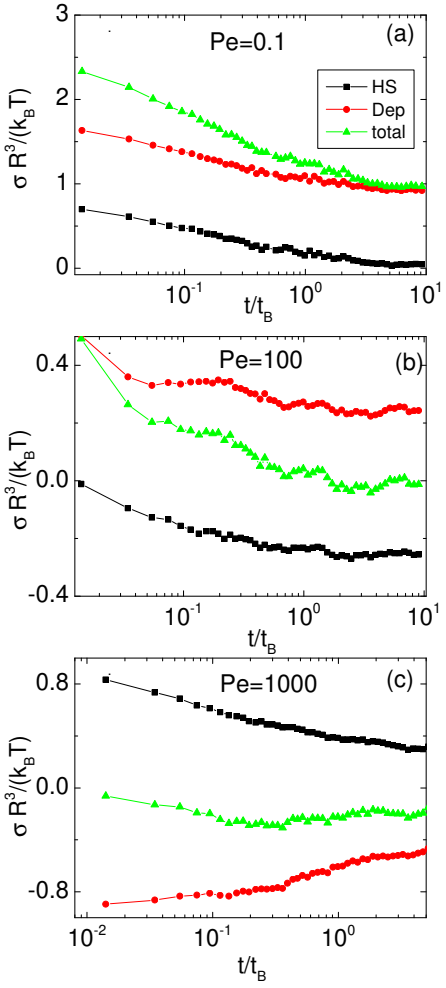

Fig. 3 Decomposition of stress into HS repulsion and depletion attractive contributions during stress relaxation of steady shear flow with $Pe =$ (a) 0.1, (b) 100, and (c) 1000 taken from BD simulations of a gel with $\phi = 0.44$, attraction range of $\xi = 0.1$ and attraction strength at contact of $U_{dep}(2R) = -20k_BT$.

peak/shoulder at large length scales comparable to several particle size, corresponds to clusters. One can calculate the average void volume as $\langle VV \rangle = \int_0^\infty P(V)VdV$ where $P(V)$ is the void volume probability density function. $\langle VV \rangle$ shown in **Fig. 4b**, exhibits a monotonic decrease with increasing Pe. Two main regimes are identified under shear: For $Pe_{dep} < 1$, $\langle VV \rangle$ is larger than the value for a quiescent thermally quenched gel indicating cluster densification under shear. In contrast for $Pe_{dep} > 1$, $\langle VV \rangle$ is smaller than in the quiescent gel indicating cluster break-up under shear. For sufficiently high Pe ($Pe_{dep} >> 1$), $\langle VV \rangle$ reaches the value for the suspension of the same volume fraction without attractions. This suggests that at such high shear rates attractive forces are essentially inactive.

We additionally examine the microstructure at more local length-scales by counting the neighboring particles within the attraction range (defined as the number of bonded particles). **Fig. 4c** shows the distribution of bonds under shear. For $Pe_{dep} > 1$, the distribution of bonds becomes narrower compared to the quiescent gel and the peak of bond distribution moves towards smaller bond

Soft Matter Accepted Manuscript

View Article Online
DOI: 10.1039/C7SM01655G

Published on 05 October 2017. Downloaded by University of Newcastle on 08/10/2017 18:22:05.

numbers. This is a result of cluster break-up under shear which leads to formation of more homogeneous structures in which particles have less number of bonds. For $Pe_{dep} < 1$, the distribution of bonds widens and the peak position moves towards larger values as a result of cluster densification under shear. In **Fig.** 4**d**, we show the average number of bonds per particle as a function of Pe. It shows similar to $\langle VV \rangle$ a monotonic decrease with increasing Pe and reaches the value obtained for a suspension of same volume fraction without attraction that essentially represent the average number of neighbors at such distance.

The decay of stress after shear cessation can be linked to the time evolution of the microstructure when gel is reformed. After flow cessation at high shear rates ($Pe_{dep} > 1$), both $\langle VV \rangle$ and the average number of bonds per particle show a strong increase with time and reach the values for the quiescent thermally quenched gel formed from a largely homogeneous liquid state. Therefore, the stress decays faster as particles are free to move and release any internal stresses. In contrast, after flow cessation from low shear rates ($Pe_{dep} < 1$), no significant change in both $\langle VV \rangle$ and the average number of bonds per particle is detected with time. Hence, the corresponding shear stress decays partially in time and leaves behind significant residual stresses.

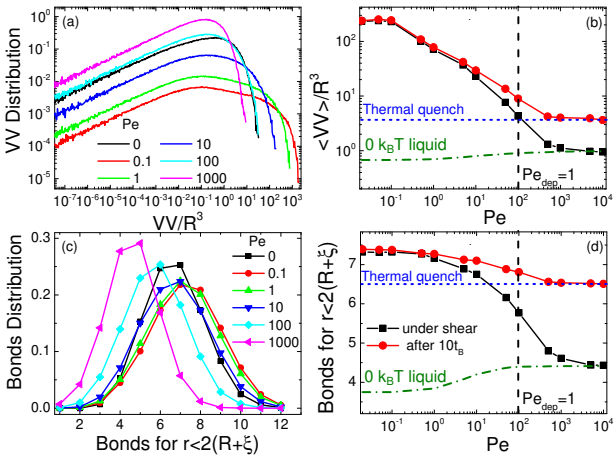

Fig. 4 (a) Void volume distribution under shear for different Pe as indicated. (b) Average void volume, $\langle VV \rangle$, as a function of Pe under steady shear (black line squares) and $10t_B$ after flow cessation (red line circles). (c) Bonds distribution under shear for different Pe as indicated. (d) Average number of bonds per particle as a function of Pe under steady shear (black line squares) and $10t_B$ after flow cessation (red line circles) taken from BD simulations with $\phi = 0.44$, $U_{dep}(2R) = -20k_BT$, $\xi = 0.1$, $Pe/Pe_{dep} = 100$. $Pe = 0$ in (a) and (c) and the blue horizontal lines in (b) and (d) represent the result at rest for the gel produced by quenching an equilibrated liquid (thermal quench). The dark green dash-dot lines in (b) and (d) show the results for the $\phi = 0.44$ without attractions.

3.3 Structural anisotropy

The examination of structural anisotropy caused by shear gives insight into the microscopic origin of the stress decay. To do this, we examine the 2D projection of the pair distribution function, $g(r)$, in the xy (velocity-gradient) plane which has a strong contribution to the shear stress (see **Eq.** 4). **Fig.** 5 shows the $g(r)$ calculated in the velocity-gradient plane under shear and also $10t_B$ after flow cessation. To enable greater clarity for structural changes, we have subtracted $g_0(r)$, describing the structure at rest, from $g(r)$[53]. We first examine structural anisotropy under shear. Application of a low shear rate (here $Pe = 0.1$, $Pe_{dep} = 0.001$) causes a small distortion in the angular symmetry of $g(r)$ (**Fig.5 a**). A clear structural anisotropy is detected at $Pe = 100$ ($Pe_{dep} = 1$) where shear and attractive forces cancel each other out (**Fig.5b**). In this case, the innermost ring of $g(r)$ reflecting the nearest neighboring structure, shows an increase of intensity in the flow direction. This indicates that particles tend to align with the flow. On the other hand, a reduction in the intensity of the first neighboring structure is seen in both the compression and the extension axes with the smallest intensity corresponding to the latter. In this case, depletion of particles in both the extension and the compression axes leads to spreading of particles to larger distances aligning them in the flow direction. However, this alignment is detected only over the first neighboring shell while at a long range, the structure is still disordered. Depletion of particles in both extension and compression axes is enhanced even further for stronger shear rates where $Pe_{dep} > 1$. This results in layering of particles in the flow direction which now has been extended to longer length scales, beyond the first neighbors (**Fig. 5c**). This is similar with the observations in concentrated HS suspensions at hight Pe, caused by the lack of hydrodynamic interactions (HI) in BD simulations[44].

We now examine the evolution of the microstructure after flow cessation. For $Pe = 0.1$, the structural anisotropy remains unchanged after switching off shear (**Fig. 5d**). In contrast, for the high Pe of 100 and 1000, a significant reduction in the intensity of the images is observed (**Fig. 5e** and **f**). For $Pe = 100$, the innermost ring of pair distribution function still shows accumulation of particles in the flow direction. Moreover, differences in the compression and extension axes have also disappeared. Although it is not obvious in the first look, a careful inspection shows an ordered distribution of intensity especially for the first neighboring shell (**Fig. 5e**). A similar response has been observed in BD simulations during flow cessation of HS glasses as well[41,42]. For $Pe = 1000$, however, one can still identify a larger value of intensity in the compression axis compared to the extension axis. One should notice that such remaining structural anisotropy at $Pe = 1000$ is indeed a consequence of the particle layering under shear, an artifact caused by the absence of HI in BD simulations.

The shear-induced structural anisotropy can be characterized through spherical harmonics expansion of the pair distribution function and calculating the coefficient $g_2^{-2}(r)$ as discussed in section 2.1. The coefficient $g_2^{-2}(r)$ quantifies the structural anisotropy in the velocity-gradient (xy) plane. Negative values of $g_2^{-2}(r)$ represent a structural anisotropy with particles being accumulated more in the compression area. Conversely, the positive values show that particles are more located in the extension axis.

The variation of $g_2^{-2}(r)$ under steady shear and also at $10t_B$ after flow cessation is shown in **Fig. 6**. The results under shear indicate two extremes: a negative minimum around $r/R = 2$ and a positive maximum at larger particle separation distances $r/R = 2.2 - 2.4$. The negative values of $g_2^{-2}(r)$ at short distances ($r/R =$

Soft Matter Accepted Manuscript

This journal is © The Royal Society of Chemistry [year]

View Article Online
DOI: 10.1039/C7SM01655G

Published on 05 October 2017. Downloaded by University of Newcastle on 08/10/2017 18:22:05.

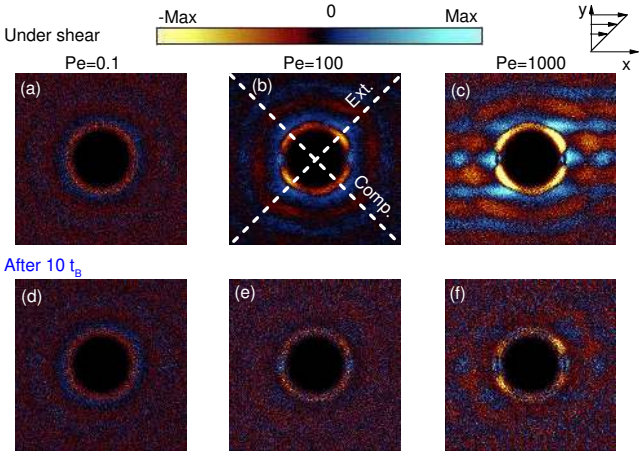

Fig. 5 The pair-distribution function projected onto the velocity-gradient (xy) plane after subtraction of the state at rest under well-developed steady shear flow of $Pe =$ (a) 0.1, (b) 100 and (c) 1000. (d), (e) and (f) are at $10t_B$ after shear cessation of $Pe = 0.1$, 100 and 1000, respectively, taken from BD simulations with $\phi = 0.44$, $U_{dep}(2R) = -20k_BT$, $\xi = 0.1$, $Pe/Pe_{dep} = 100$. Dashed lines in (b) indicate extension and compression axes. The direction of shear field along with the color scale are also indicated.

2) suggest that under shear particles come into contact in the compression axis while the positive values at larger distances exhibit that particles are pushed out in the extension axis. A clear increase of both the depth of minimum and the height of maximum is detected with increasing Pe. This indicates an increase of structural anisotropy with Pe in the velocity-gradient plane due to an increase of accumulation and depletion of particles in compression and extension axes, respectively.

Upon flow cessation, however, both the depth of the minimum and the height of the maximum show a decrease indicating the reduction in the angular asymmetry of the pair distribution function. After shear cessation of a low Pe, the structural anisotropy persist after $10t_B$ although it has reduced (**Fig. 6a**). As the shear stress is directly related to structural anisotropy in the xy plane (see **Eq.** 4), one can argue that the residual stresses observed at low Pe are due to the persistence of such shear-induced structural anisotropy. To the contrary for $Pe = 100$, both the minimum and maximum of the $g_2^{-2}(r)$ relax to zero after shear cessation (**Fig. 6b**). Therefore, based on the **Eq.** 4, the corresponding residual stresses diminish with $\sigma^{HS} = -\sigma^{Dep}$ as is seen in **Fig. 3b**. On the other hand for $Pe = 1000$, the depth of minimum decreases to a non-zero value while the height of the maximum reduces to almost zero (**Fig. 6c**). Therefore, the negative values of shear stress observed in **Fig. 3 c** is due to persistence of structural anisotropy mainly in the compression area where repulsive forces are contributing positively to the stress (due to negative $g_2^{-2}(r)$ and positive $\frac{dU^{HS}}{dr}$) while the attractive forces negatively (due to both negative $g_2^{-2}(r)$ and $\frac{dU^{Dep}}{dr}$) in agreement with findings in **Fig. 3c**.

Related to the above, the negative values of shear stresses observed after shear cessation at high Pe is an artifact due to absence of HI in BD simulations. As attractions are inactive during sufficiently high shear rates the shear melted gel has the same structural properties with a hard-sphere suspension at the same volume fractions (manifested by particle layering in the absence of HI). When shear is switched off, in the case of suspension with no attractions, stresses are completely released as an isotropic structure is recovered by Brownian motions. In a gel, however, when shear is switched off, attractions are becoming active preventing the layered structure to relax towards the quiescent structure, as gel is frozen quickly. We thus expect that if full HI is implemented, the gel should recover to a rather isotropic structure after shear cessation of high shear rates (since no layering would be present under shear) in agreement with experimental results.

Another important finding is that in BD simulations, the gel prepared through shear cessation at high Pe has the same averaged structural length-scale properties as the one obtained through thermal quench when is interrogated by $\langle VV \rangle$ and the average number of bonds per particle (**Fig. 4b** and **d**). However, a difference between the two gel states can be identified by a quantification of the structural anisotropy. As has been shown in **Fig. 6**, the gel obtained through a thermal quench is isotropic ($g_2^{-2}(r) = 0$) while the one prepared by shear cessation at very high Pe is largely anisotropic. However, as mentioned earlier, the remained structural anisotropy after switching off shear at such very high Pe, is due to layering of particles in the absence of HI in BD simulations.

3.4 Particle scale dynamics

The physical picture of stress relaxation can be complemented through examination of particle dynamics. As during stress relaxation, the system is not at steady state, the time-averaged mean squared displacement (MSD) cannot provide information on the transient dynamics and the relevant microstructural changes. Hence, we evaluate the two-time mean-squared displacement as a function of $(t - t_w)$ with t_w the waiting time from the onset of flow cessation:

$$\left\langle \Delta r^2(t, t_w) \right\rangle_N = \frac{1}{N} \sum_{i=1}^{N} [r_i(t + t_w) - r_i(t_w)]^2 \qquad (6)$$

Here, we report the MSDs measured in the vorticity direction as similar response is also detected in the velocity and gradient directions after subtracting the affine motion due to shear. **Fig.** 7 shows two-time MSDs calculated in the vorticity direction. The t_w independent MSD at rest and under steady shear are also shown as a reference. The MSD at rest exhibits a sub-diffusive response at short times while the long-time dynamics are frozen as particles are trapped in the gel network with the localization length (defined as the maximum particle displacement or equivalently the plateau in MSD) much smaller than the attraction range (of $\xi = 0.1$,) similarly to the case of attractive glasses[56]. The application of steady shear results in the emergence of a long-time mobility as shear assists particles to escape their attractive bonds. The MSD immediately after shear cessation, $t_w = 0$, shows an intermediate response between that under shear and the quiescent state. At short times, it follows the MSD under shear, but as the time passes, the MSD values deviate from that under shear

Soft Matter Accepted Manuscript

View Article Online
DOI: 10.1039/C7SM01655G

Published on 05 October 2017. Downloaded by University of Newcastle on 08/10/2017 18:22:05.

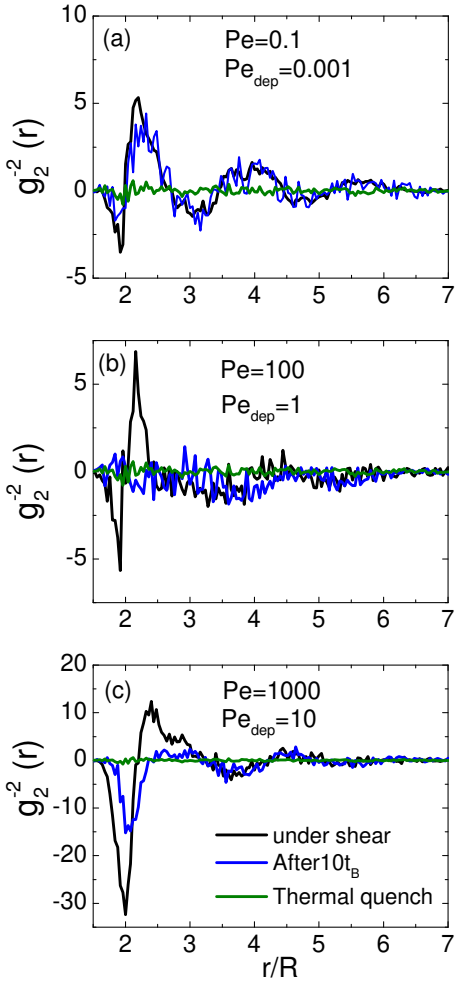

Fig. 6 The values of $g_2^{-2}(r)$ for steady shear (black curves) and at $10t_B$ after shear cessation (blue curves) of $Pe =$ (a) 0.1, (b) 100, and (c) 1000 taken from BD simulations with $\phi = 0.44$, $U_{dep}(2R) = -20k_BT$, $\xi = 0.1$, $Pe/Pe_{dep} = 100$. The green line represents the result at rest for the gel produced by quenching an equilibrated liquid (thermal quench).

following a sub-diffusive dynamic which at long-time reaches a plateau.

One can relate the short-time stress decay to this sub-diffusive particle displacements over short distances which reduces the asymmetry of the pair distribution function caused during the course of shear. This scenario of stress decay is similar with HS glasses[9] and differs from jammed soft particle suspensions where ballistic motions are detected during initial stress decay[10,11]. The transient long-time dynamics are arrested as the particles are trapped in the network with the localization length larger than in the quiescent state but still smaller than the attraction range. Hence, particles are not able to undergo long-range motions that will allow large-scale rearrangements at length scales of the order or larger than the particle size (or first neighbors). Therefore under such conditions, some structural anisotropy persists which is more prominent at low Pe creating frozen-in stresses. The complete picture emerges when the MSD as a reference to the cessation point, $t_w = 0$, at different shear rates is examined. For all shear rates, the dynamics at intermediate times are sub-diffusive while long-time dynamics are frozen (**Fig. 7b**). However, faster and larger particle rearrangements are taking place after shear cessation at higher shear rates which leads to the stronger and faster stress decay after flow cessation (**Fig. 2**). For $Pe_{dep} < 1$ where residual stresses are present, the maximum particle displacement is smaller than the attraction range. In contrast, for $Pe_{dep} > 1$, where stresses are released completely, the localization length exceeds the attraction range. Hence, one can use particle mobility at the length scale of the localization length as a dynamic measure (or signature) of how much internal stresses will relax in colloidal gels.

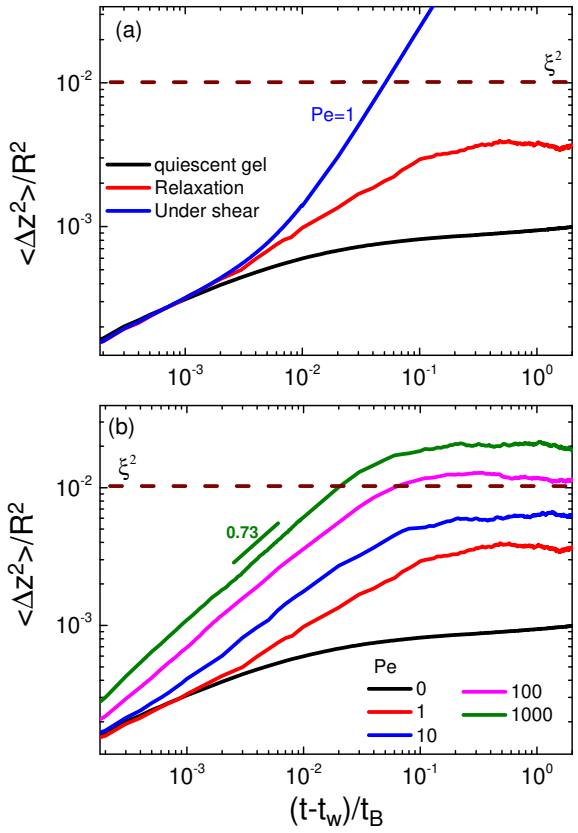

Fig. 7 Mean-squared displacement (MSD) in the vorticity direction starting at the waiting time $t_w = 0$ after onset of flow cessation taken from BD simulations with $\phi = 0.44$, $U_{dep}(2R) = -20k_BT$ and $\xi = 0.1$. (a) MSD after flow cessation of $Pe = 1$ together with the steady-state shear and quiescent state result, as indicated. (b) MSD upon flow cessation at different shear rates, as indicated. $Pe = 0$ denotes the quiescent state for the thermally quenched gel. The horizontal brown dashed lines represent $\xi^2 = 0.01$.

3.5 Scaling of residual stresses

We finally examine the effect of inter-particle attraction strength on the residual stresses. **Fig. 8a** shows residual stresses at $10t_B$ after flow cessation as a function of Pe, for different attraction strengths from both BD simulations and experiments. At a fixed Pe, the gel with the higher attraction strength exhibits larger residual stresses after flow cessation. On the other hand, less bond breaking under shear takes place for the gel with higher attraction strength[29]. This means that residual stresses are controlled

Soft Matter Accepted Manuscript

This journal is © The Royal Society of Chemistry [year]

View Article Online
DOI: 10.1039/C7SM01655G

Published on 05 October 2017. Downloaded by University of Newcastle on 08/10/2017 18:22:05.

by how much shear is able to break the bonds between the particles. Therefore, plotting residual stresses versus Pe_{dep} which takes into account such competition between shear and attractive forces should lead to a universal curve for different attraction strengths. **Fig. 8b** shows such scaling with Pe_{dep}. Indeed all curves collapse onto a mastercurve, indicating that the amount of residual stresses in colloidal gels is a unique function of the ratio of shear to the attractive forces quantified by Pe_{dep}. Experimental data show almost equal magnitude of residual stresses with the simulations for each Pe and therefore collapse on the same mastercurve as well.

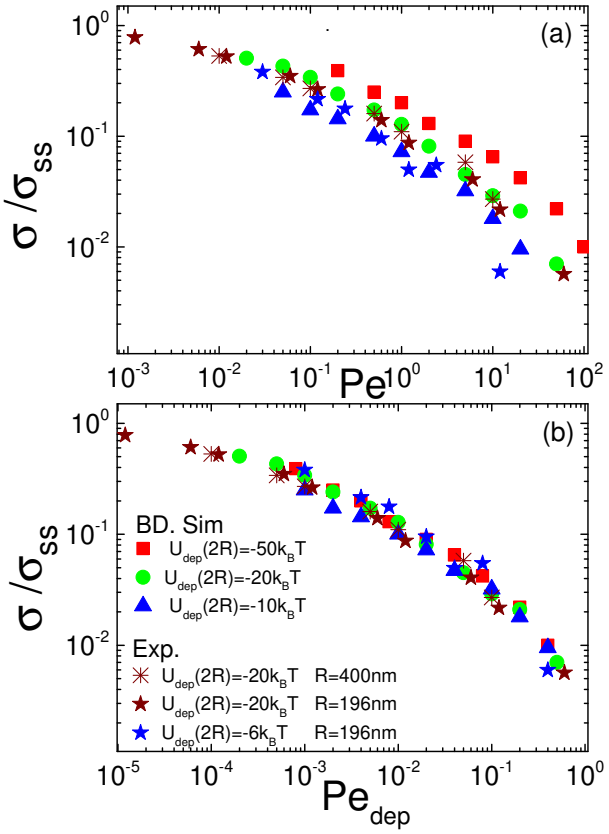

Fig. 8 Residual stresses at $t = 10t_B$ after shear cessation as a function of (a) Pe and (b) Pe_{dep}. Experiments performed for particles with $R = 400\ nm$, $U_{dep}(2R) = -20k_BT$, $\xi = 0.09$ and $R = 196\ nm$ with $U_{dep}(2R) = -6$ and $-20k_BT$, $\xi = 0.1$. In simulations, $U_{dep}(2R) = -10, -20, -50k_BT$ as indicated with $\xi = 0.1$.

4 Conclusions

We used experimental rheometry and BD simulations to investigate the stress relaxation after flow cessation of a well-defined steady shear flow for an intermediate volume fraction colloidal gel. The dimensionless number, Pe_{dep}, defined as the ratio of shear forces to attractive forces is used to rationalize the transition from low to high shear rates. Analysis of the structure under shear reveals two distinct regimes. Under high shear rates, $Pe_{dep} > 1$, where shear forces are stronger than attractive forces, the shear-melted gel behaves as a viscoelastic liquid due to extensive cluster break-up. In contrast for low shear rates ($Pe_{dep} < 1$), cluster densification under shear takes place. Moreover, shear causes an asymmetry in the angular dependence of the pair distribution function due to accumulation and depletion of particles in the compression and extension axes, respectively. These two distinct regimes of shearing relate with two well-defined patterns of stress decay after flow cessation: For high shear rates ($Pe_{dep} > 1$) stresses are released fully similar to liquids, as particles are free to move and therefore enable local stress relaxation before they are trapped in a network. On the other hand, at low shear rates ($Pe_{dep} < 1$) only weak structural changes are observed after flow cessation and stresses do not decay much with time, similarly to the case of HS glasses.

Microscopically, BD simulations suggest that when shear is stopped, particles move sub-diffusively over short distances reducing the shear-induced anisotropy detected in the pair distribution function which leads to the initial stress decay. For low Pe ($Pe_{dep} < 1$) where frozen-in stresses are observed, the maximum particle displacement is smaller than the attraction range which is not sufficient to completely erase the shear-induced structural anisotropy. At high Pe ($Pe_{dep} > 1$) though, particles may move at distances similar or larger than the attraction range allowing enough rearrangements to erase anisotropy and fully relax internal stresses.

Our results demonstrate that the inter-particle attraction strength and the shear rate during the steady state flow are the decisive factors controlling internal stresses in colloidal gels. A stronger preshear and/or weaker attractions result into lower residual stresses after shear cessation due to larger structural distortion under shear. Remarkably, these two factors are described adequately by Pe_{dep} leading to a universal scaling for internal stresses in colloidal gels. Our results provide in-depth understanding of residual stresses and the way that they can be manipulated in a well-defined model soft matter system with tunable isotropic short-range attractions. This may be useful in understanding and predicting residual stresses build-up after shear cessation (or equivalently after processing) in many complex multicomponent materials and commercial soft matter products where attractions between constituents are ubiquitous.

5 Acknowledgments

We thank A. B. Schofield (University of Edinburgh) for providing the PMMA particles, Nick Koumakis and Benoit Loppinet for helpfull discussions. The work was supported by Greek projects Thales "Covisco", Aristeia II "MicroSoft" and EU project "Smart-Pro".

References

1 J. Mewis and N. J. Wagner, *Colloidal Suspension Rheology*, Cambridge University Press, 2012.
2 L. Struik, *Internal stresses, dimensional instabilities, and molecular orientations in plastics*, Wiley, 1990.
3 L. Ramos and L. Cipelletti, *Phys. Rev. Lett.*, 2001, **87**, 245503.
4 L. Ramos and L. Cipelletti, *Phys. Rev. Lett.*, 2005, **94**, 158301.
5 S. Mazoyer, L. Cipelletti and L. Ramos, *Phys. Rev. Lett.*, 2006, **97**, 238301.
6 O. Lieleg, J. Kayser, G. Brambilla, L. Cipelletti and A. Bausch,

Soft Matter Accepted Manuscript

View Article Online
DOI: 10.1039/C7SM01655G

Published on 05 October 2017. Downloaded by University of Newcastle on 08/10/2017 18:22:05.

Nature Materials, 2011, **10**, 236–242.
7 G. Reiter, M. Hamieh, P. Damman, S. Sclavons, S. Gabriele, T. Vilmin and E. Raphaël, *Nature Materials*, 2005, **4**, 754.
8 T. Narita, C. Beauvais, P. Hébraud and F. Lequeux, *The European Physical Journal E*, 2004, **14**, 287.
9 M. Ballauff, J. M. Brader, S. U. Egelhaaf, M. Fuchs, J. Horbach, N. Koumakis, M. Krüger, M. Laurati, K. J. Mutch, G. Petekidis, M. Siebenbürger, T. Voigtmann and J. Zausch, *Physical Review Letters*, 2013, **110**, 215701.
10 L. Mohan, R. T. Bonnecaze and M. Cloitre, *Phys. Rev. Lett.*, 2013, **111**, 268301.
11 L. Mohan, M. Cloitre and R. T. Bonnecaze, *Journal of Rheology*, 2015, **59**, year.
12 C. O. Osuji, C. Kim and D. A. Weitz, *Phys. Rev. E*, 2008, **77**, 060402.
13 A. S. Negi and C. O. Osuji, *Rheologica acta*, 2009, **48**, 871–881.
14 A. S. Negi and C. O. Osuji, *Journal of Rheology (1978-present)*, 2010, **54**, 943–958.
15 L. Cipelletti and L. Ramos, *Journal of Physics: Condensed Matter*, 2005, **17**, R253.
16 L. Cipelletti, S. Manley, R. Ball and D. Weitz, *Physical review letters*, 2000, **84**, 2275.
17 M. Bouzid, J. Colombo, L. V. Barbosa and E. Del Gado, *Nature communications*, 2017, **8**, year.
18 D. Green, R. Tandon and V. Sglavo, *Science*, 1999, **283**, 1295–1297.
19 Y. Zhang, W. Wang and A. Greer, *Nature Materials*, 2006, **5**, 857–860.
20 Y. Cao, X. Xie, J. Antonaglia, B. Winiarski, G. Wang, Y. C. Shin, P. J. Withers, K. A. Dahmen and P. K. Liaw, *Scientific reports*, 2015, **5**, year.
21 S. Asakura and F. Oosawa, *The Journal of Chemical Physics*, 1954, **22**, 1255–1256.
22 W. C. K. Poon, *Journal of Physics: Condensed Matter*, 2002, **14**, R859.
23 K. N. Pham, G. Petekidis, D. Vlassopoulos, S. U. Egelhaaf, W. C. K. Poon and P. N. Pusey, *Journal of Rheology*, 2008, **52**, 649–676.
24 M. Laurati, S. U. Egelhaaf and G. Petekidis, *Journal of Rheology*, 2011, **55**, 673–706.
25 N. Koumakis, M. Laurati, S. U. Egelhaaf, J. F. Brady and G. Petekidis, *Physical Review Letters*, 2012, **108**, 098303.
26 Z. Shao, A. S. Negi and C. O. Osuji, *Soft Matter*, 2013, **9**, 5492–5500.
27 M. Laurati, S. U. Egelhaaf and G. Petekidis, *Journal of Rheology*, 2014, **58**, year.
28 E. Moghimi, A. R. Jacob, N. Koumakis and G. Petekidis, *Soft Matter*, 2017, **13**, 2371–2383.
29 N. Koumakis, E. Moghimi, R. Besseling, W. C. K. Poon, J. F. Brady and G. Petekidis, *Soft Matter*, 2015, **11**, 4640–4648.
30 R. C. Sonntag and W. B. Russel, *Journal of colloid and interface science*, 1987, **115**, 390–395.
31 J. C. Conrad and J. A. Lewis, *Langmuir*, 2008, **24**, 7628–7634.
32 K. Masschaele, J. Fransaer and J. Vermant, *Journal of Rheology*, 2009, **53**, 1437–1460.
33 L. C. Hsiao, R. S. Newman, S. C. Glotzer and M. J. Solomon, *Proceedings of the National Academy of Sciences*, 2012, **109**, 16029–16034.
34 B. Rajaram and A. Mohraz, *Soft Matter*, 2012, **8**, 7699.
35 J. D. Park and K. H. Ahn, *Soft Matter*, 2013, **9**, 11650–11662.
36 H. Chen, M. A. Fallah, V. Huck, J. I. Angerer, A. J. Reininger, S. W. Schneider, M. F. Schneider and A. Alexander-Katz, *Nature Communications*, 2013, **4**, 1333.
37 P. Ballesta, N. Koumakis, R. Besseling, W. C. K. Poon and G. Petekidis, *Soft Matter*, 2013, **9**, 3237–3245.
38 J. D. Park, K. H. Ahn and S. J. Lee, *Soft Matter*, 2015, **11**, 9262–9272.
39 D. Aarts, R. Tuinier and H. Lekkerkerker, *Journal of Physics: Condensed Matter*, 2002, **14**, 7551.
40 G. J. Fleer and R. Tuinier, *Physical Review E*, 2007, **76**, 041802.
41 N. Koumakis, *PhD thesis*, Department of Materials Science and Technology, University of Crete, 2011.
42 A. R. Jacob, *PhD thesis*, Department of Materials Science and Technology, University of Crete, 2016.
43 D. Heyes and J. Melrose, *Journal of Non-Newtonian Fluid Mechanics*, 1993, **46**, 1 – 28.
44 D. R. Foss and J. F. Brady, *Journal of Rheology*, 2000, **44**, 629–651.
45 A. Sierou and J. F. Brady, *Journal of Fluid Mechanics*, 2001, **448**, 115–146.
46 H. J. M. Hanley, J. C. Rainwater and S. Hess, *Phys. Rev. A*, 1987, **36**, 1795–1802.
47 S. Hess and H. Hanley, *International Journal of Thermophysics*, 1983, **4**, 97–114.
48 N. J. Wagner and B. J. Ackerson, *The Journal of Chemical Physics*, 1992, **97**, 1473–1483.
49 H. Hanley, J. Rainwater and S. Hess, *Physical Review A*, 1987, **36**, 1795.
50 J. Rainwater, H. Hanley and S. Hess, *Physics Letters A*, 1988, **126**, 450 – 454.
51 J. R. Seth, L. Mohan, C. Locatelli-Champagne, M. Cloitre and R. T. Bonnecaze, *Nature Materials*, 2011, **10**, 838–843.
52 J. D. Park, K. H. Ahn and N. J. Wagner, *Journal of Rheology*, 2017, **61**, 117–137.
53 N. Koumakis, M. Laurati, A. Jacob, K. Mutch, A. Abdellali, A. Schofield, S. Egelhaaf, J. Brady and G. Petekidis, *Journal of Rheology (1978-present)*, 2016, **60**, 603–623.
54 A. P. R. Eberle, N. Martys, L. Porcar, S. R. Kline, W. L. George, J. M. Kim, P. D. Butler and N. J. Wagner, *Physical Review E*, 2014, **89**, 050302.
55 J. Min Kim, A. P. Eberle, A. Kate Gurnon, L. Porcar and N. J. Wagner, *Journal of Rheology*, 2014, **58**, 1301–1328.
56 E. Moghimi, *PhD thesis*, Department of Materials Science and Technology, University of Crete, 2016.

Soft Matter Accepted Manuscript

This journal is © The Royal Society of Chemistry [year]